Journal of Photochemistry, 3 (1974/75) 27 - 36

KINETICS OF EXCITED MOLECULES
VII. PHOTOCHEMISTRY OF HEXAFLUOROBIACETYL VAPOUR

GERALD B. PORTER and WILLIAM J. REID*

Department of Chemistry, University of British Columbia, Vancouver 8, British Columbia, (Canada)

(Received November 2, 1973)

Summary

The photodecomposition of hexafluorobiacetyl into C_2F_6 and 2 CO has been studied in the vapour at seven wavelengths from 254 to 436 nm as a function of pressure from 1 to 400 Torr. Dissociation occurs from two different electronic states, most likely the second excited singlet and triplet states. No decomposition occurs from either the lowest excited singlet state or from low vibronic levels of the lowest triplet state. Evidence is presented for a strong energy dependence for both photodissociation and intersystem crossing.

Introduction

Although the photophysics and photochemistry of biacetyl have been studied extensively and are moderately well understood [1], the details of the primary photoprocesses are partly obscured by the chemical complexity of the system. A complete material balance has not been obtained from the experimental data, so that assumptions must be made about supposed products in order to estimate the primary photochemical quantum yields [2]. Just as hexafluoroacetone provides a photochemically simpler analogue to acetone [3], hexafluorobiacetyl also allows a more direct evaluation of the primary processes than does biacetyl. Fluorine is not readily abstracted at temperatures below 500 K [4], and the trifluoroacetyl radical is unstable with respect to dissociation into trifluoromethyl and carbon monoxide [5].

While the photophysical processes of both biacetyl [6] and hexafluorobiacetyl [7] have been studied over a wide range of conditions, including the low pressures essential to such studies, the photochemical processes for biacetyl have only been studied down to about 10 Torr [2], in part because of the chemical complexity. There are no such barriers to extended studies of

* Present address: Uniroyal Ltd, Research Laboratories, Guelph, Ontario N1H 6N3 (Canada).

hexafluorobiacetyl. In the following, we report a detailed study of the photochemistry of hexafluorobiacetyl including the effects of wavelength, pressure and temperature.

Experimental

Hexafluorobiacetyl (HFB) was prepared by the chromic acid oxidation of 2,3-dichloro-1,1,4,4,4-hexafluoro-2-butene [5]. The crude condensate was partly purified by trap-to-trap distillation *in vacuo* from −78 °C (methanol/CO_2) to −96 °C (toluene/liquid N_2) slush baths. This procedure was repeated several times. The majority of this semi-pure material was stored in break-seals at −78 °C. The portion of hexafluorobiacetyl to be used in the series of experiments was further purified by distillation through a Le Roy–Ward still set at −65 °C and then stored in the side arm of a blackened 1 litre globe at −196 °C. Immediately prior to use the sample was degassed at −196 °C. A phosphorescence lifetime determination served as a criterion of adequate degassing. Hexafluoroethane, Matheson Co. Freon 116, was degassed at −196 °C by trap-to-trap distillation. Carbon monoxide, supplied by Matheson Co. (C.P. grade) was used without further purification. Hexafluoroazomethane (Merck, Sharp and Dohme, Montreal) was degassed at −196 °C by trap-to-trap distillation.

A completely mercury-free vacuum system was used for all the experiments. Pressures greater than 20 Torr were measured directly with a calibrated glass spiral gauge. Lower pressures were obtained by expansion into calibrated volumes on the vacuum line. High vacuum Teflon stopcocks (Kontes, Vineland, New Jersey) were used on the cells and throughout the analytical section of the apparatus.

Photolysis was carried out in either of two cylindrical Pyrex cells. Both cells had an internal diameter of 20 mm and were fitted with quartz windows by Araldite resin. One of the cells, 30 cm long, had a water jacket for temperature controlled runs. The other cell, 5 cm long, was attached to a glass magnetically driven mixing chamber. Thirty minutes in this cell was found adequate to ensure a completely homogeneous sample of gas mixture. A quartz window was fitted to one side of the short cell with Araldite in order to monitor emission.

The excitation source was a PEK 110 mercury arc lamp operated at 100 W from a stabilized d.c. power supply (PEK Model 401). A Bausch and Lomb Monochromator (33-86-25) was used for isolation of the exciting wavelengths. They were the 436, 405, 366, 334, 313, 297 and 254 nm Hg lines. With 254 nm radiation the exit slit was set at 3.0 mm, while at all other wavelengths, the exit slit width was 1.0 mm. The divergent beam from the monochromator was passed through a combination of two quartz plano-convex lenses which produced a parallel beam of radiation.

A Corning 7-54 visible absorbing filter was used in the exciting beam at 254, 297, 313, 334 and 366 nm. At 405 nm and 436 nm Corning 3-75 and Corning 3-73 filters were used respectively.

The intensity of light was measured *before* it entered the cell by having a quartz window in the optical train set at an angle so as to reflect some light onto an RCA 935 phototube. This phototube had been previously calibrated by ferrioxalate actinometry. The intensity of light was also measured by a different phototube *after* it traversed the cell. This latter detector was used primarily to determine the fraction of light absorbed (*in situ*) for each photolysis run.

The techniques used for phosphorescence lifetime measurements and for detecting and recording the emission spectra have been described [7].

After photolysis the contents of the reaction cell were allowed to flow through two successive traps at —196 °C (liquid N_2). These condensed out C_2F_6 and unchanged substrate; carbon monoxide was measured as the only non-condensable product. One re-evaporation of the condensed products was necessary to release occluded CO. The latter was then transferred by a Delmar–Urry Automatic Topler Pump to a small sampling chamber. The carrier gas of the chromatograph was then diverted through the chamber so that the CO was flushed onto the chromatographic column. The latter was a 5 ft. × 0.25 in. molecular sieve solumn (13X) operated at 100 °C and at a flow of 75 ml/min. The detector was a Varian Aerograph thermal conductivity detector (No. 01-000334-00) with two matched pairs of 30 Ω tungsten rhenium (WX) filaments. They were operated at 150 mA and at ambient temperature. The power supply was a Kepco regulated d.c. supply (Model PAT 21-1T). The chromatograph was calibrated using known samples of CO after each run. For the ratio of CO to C_2F_6 the contents of the cell were expanded into an evacuated sample loop. The sample was subsequently flushed onto a 5 ft. × 0.25 in. Porapak Q (50 - 80 mesh) column operated at 0 °C and a flow of 75 ml/min. The chromatograph was calibrated using known synthetic mixtures.

Results

The quantum yields of carbon monoxide and hexafluoroethane were found to be in the ratio of 2 to 1. On this basis, therefore, only carbon monoxide was determined thereafter for each photolysis run. The photochemical data are presented in Fig. 1 and 2 which show the reciprocal primary quantum yield ($\frac{1}{2}\,\Phi_{CO}$) as a function of pressure of HFB for a variety of excitation wavelengths at room temperature. Figure 3 shows the effect of temperature on the quantum yield. Table 1 gives upper limits for the photochemical quantum yields with 405 and 436 nm radiation. No products were detected at these wavelengths. Table 2 summarizes the results obtained by photolyzing hexafluorobiacetyl–hexafluoroazomethane mixtures in which the phosphorescence of the former is completely quenched by the latter. No effect on the photochemical quantum yield could be detected.

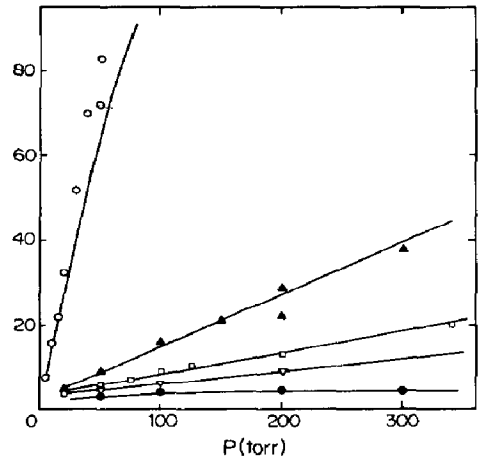

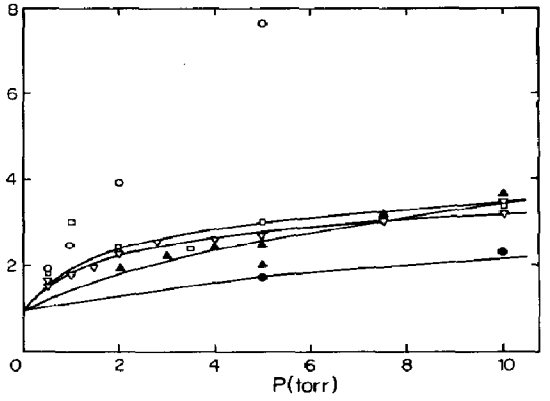

Fig. 1. Reciprocal quantum yields as a function of perfluorobiacetyl pressure at the wavelengths: ○, 366; ▲, 334; □, 313; ▽, 297; and ●, 254 nm, at 25 °C.

Fig. 2. Reciprocal primary quantum yields at low pressures of perfluorobiacetyl at the same wavelengths as in Fig. 1.

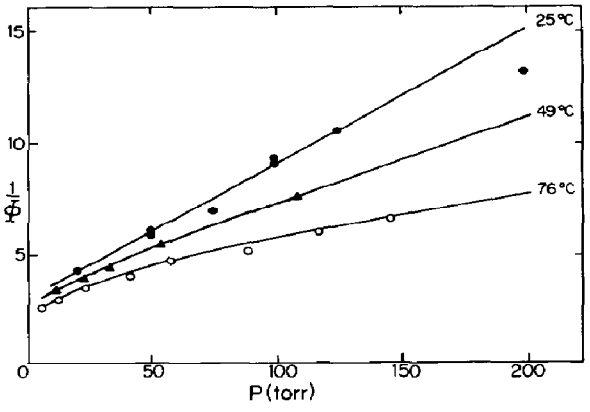

Fig. 3. Temperature dependence of the primary quantum yields at 313 nm.

TABLE 1

Long wavelength photolysis of hexafluorobiacetyl at 25 °C

λ/nm	Pressure/Torr	Φ
405	1.0	< 0.0019
405	2.0	< 0.0016
436	0.5	< 0.0014
436	2.0	< 0.0007
436	5.0	< 0.0003

TABLE 2

Photolysis of hexafluorobiacetyl in the presence of hexafluoroazomethane at 25 °C and 297 nm

Pressure of hexafluorobiacetyl/Torr	Pressure of hexafluoroazomethane/Torr	Φ
0.5	1.5	0.44
2.0	0	0.43
10.0	0.2	0.29
10.0	0	0.31
45.7	0.2	0.19
50.0	0	0.20
100	0.2	0.17
100	0	0.15

Discussion

The absorption spectrum of hexafluorobiacetyl vapour in the visible and near u.v. is almost identical with that of biacetyl itself in shape, position and intensity of the bands observed. It has three main bands assigned as [9, 10]: $^1A_u \leftarrow {}^1A_g$, $\lambda_{max} = 410$ nm, $\epsilon = 15$; $^1A_u \leftarrow {}^1A_g$, $\lambda_{max} = 290$ nm, $\epsilon = 17$; and $^1B_u \leftarrow {}^1A_g$, $\lambda_{max} = 200$ nm, $\epsilon = 109\ M^{-1}\ cm^{-1}$. The first two absorption bands [8] have some diffuse structure. Because of low intensity, no transitions from the ground singlet state to triplet states have been located in absorption.

Both the fluorescence and phosphorescence of hexafluorobiacetyl are slightly red-shifted from the corresponding emissions of biacetyl [8]. The fluorescence, $\lambda_{max} = 475$ nm, has no structure, but the phosphorescence, $\lambda_{max} = 537$ nm, shows several broad bands with a spacing of 1650 cm^{-1}. The lifetime of the lowest triplet state, measured by phosphorescence decay, is 1.93 ms. The luminescence quantum yields are [7]: $\Phi_p = 0.078$ and $\Phi_f = 4.8 \times 10^{-3}$. These data are comparable to those of biacetyl except that the ratio of phosphorescence to fluorescence is about 16 for hexafluorobiacetyl as compared with 60 for biacetyl.

Although the luminescence behavior will be described separately [7], it is appropriate to outline here the pertinent experimental data for hexafluorobiacetyl. To emphasize the relation between luminescence and photochemistry, the corresponding features are listed together:

(i) At any given wavelength $\lambda < 400$ nm, as the pressure is increased:
  (a) the quantum yields of fluorescence (Φ_f) and of phosphorescence (Φ_p) increase,
  (b) the photochemical primary quantum yield (Φ) decreases.

(ii) At all wavelengths $\lambda < 400$ nm, in the limit of high pressure:
  (a) Φ_f and Φ_p approach the limiting values, Φ_f^∞ and Φ_p^∞, respectively,
  (b) Φ approaches zero.

(iii) At any given pressure, as the excitation wavelength is decreased:
(a) Φ_f and Φ_p decrease,
(b) Φ increases.

(iv) For excitation in the long wavelength part of the absorption spectrum, $\lambda \geqslant 400$ nm:
(a) Φ_f and Φ_p have the constant values of Φ_f^∞ and Φ_p^∞, independent of pressure,
(b) Φ is essentially zero.

(v) At low pressures:
(a) the ratio Φ_p/Φ_f goes through a maximum value, and approaches zero at zero pressure,
(b) Φ is larger than expected based on extrapolation from high pressure, and approaches one at zero pressure.

(vi) Small amounts of hexafluoroazomethane:
(a) quench the phosphorescence without appreciable effect on the fluorescence,
(b) have no quenching effect on Φ.

All of these data can be rationalized in terms of a mechanism involving two excited electronic states with vibrational energy in excess of equilibrium. The simplest mechanism is the following:

$B + h\nu$	$\rightarrow {}^1B^*$	I_a	(1)
${}^1B^*$	$\rightarrow {}^3B^*$	$k_i^*[{}^1B^*]$	(2)
${}^1B^*$	$\rightarrow$ products	$k_s[{}^1B^*]$	(3)
${}^1B^*$	$\rightarrow B + h\nu_f$	$k_f[{}^1B^*]$	(4)
${}^1B^* + M$	$\rightarrow {}^1B^\circ + M^*$	$\omega[M][{}^1B^*]$	(5)
${}^1B^\circ$	$\rightarrow {}^3B^\circ$	$k_i[{}^1B^\circ]$	(6)
${}^1B^\circ$	$\rightarrow B + h\nu_f$	$k_f[{}^1B^\circ]$	(7)
${}^3B^*$	$\rightarrow$ products	$k_t[{}^3B^*]$	(8)
${}^3B^* + M$	$\rightarrow {}^3B^\circ + M^*$	$\omega[M][{}^3B^*]$	(9)
${}^3B^\circ$	$\rightarrow B + h\nu_p$	$k_p[{}^3B^\circ]$	(10)
${}^3B^\circ$	$\rightarrow B^*$	$k_d[{}^3B^\circ]$	(11)

The rates of each elementary reaction are given next to the chemical equations. The superscript * denotes excess vibrational energy, while the superscript $^\circ$ signifies a species in thermal equilibrium with the medium in every sense except that of electronic excitation.

By straightforward application of a steady-state analysis for the species: ${}^1B^*$, ${}^1B^\circ$, ${}^3B^*$ and ${}^3B^\circ$, the following expressions are obtained for the quantum yields:

$$\Phi_f = \frac{k_f}{(k_i^* + k_s + k_f + \omega[M])}\left(1 + \frac{\omega[M]}{k_i + k_f}\right) \tag{12}$$

$$\Phi_p = \frac{k_p \omega[M]}{(k_p + k_d)(k_i^* + k_s + k_f + \omega[M])}\left(\frac{k_i}{k_i + k_f} + \frac{k_i^*}{k_t + \omega[M]}\right) \tag{13}$$

$$\Phi = \frac{1}{(k_i^* + k_s + k_f + \omega[M])}\left(k_s + \frac{k_i^* k_t}{k_t + \omega[M]}\right) \tag{14}$$

Each of these quantum yield equations consists of a sum of two terms. For the fluorescence, the first and second terms represent emission from vibrationally excited and equilibrated levels, respectively, of the lowest singlet state. In the equation for the phosphorescence, the first term is for those molecules reaching $^3B^0$ *via* intersystem crossing, eqn. (6), after equilibration of $^1B^*$ to $^1B^0$, eqn. (5). The second term concerns those molecules reaching $^3B^0$ by equilibration of $^3B^*$ after intersystem crossing from $^1B^*$, eqn. (2). The emission of $^3B^*$ itself is ignored because $k_p(\approx 40\ s^{-1})$ is too small for phosphorescence to compete with vibrational relaxation at $p = 1$ Torr. The two terms in eqn. (14) represent dissociation of $^1B^*$ and $^3B^*$, respectively. It must be assumed that neither $^1B^0$ nor $^3B^0$ are capable of dissociation.

An additional step is required in the mechanism if hexafluoroazomethane is present:

$$^3B^0 + A \rightarrow B + {}^3A^0 \qquad k_{et}[A][^3B^0] \tag{15}$$

The denominator of eqn. (13) then includes a term $k_{et}[A]$; however, eqns. (12) and (14) are unaffected.

Equation (14) has the form:

$$\Phi = \frac{(1 + a[M])}{(1 + b[M])\,(1 + c[M])} \tag{16}$$

The data can be fitted to this equation with a weighted non-linear least squares analysis [11] to evaluate a, b and c. Comparison of eqns.(16) and (14) shows that:

$$k_s = \frac{a\omega}{bc} \tag{17a}$$

$$k_i^* = \frac{\omega}{b}\left(1 - \frac{a}{c}\right) \tag{17b}$$

$$k_t = \frac{\omega}{c} \tag{17c}$$

Physically real solutions are obtained only if $c > a$. For example, at 313 nm, the best fit to eqn. (16) is:

$$\Phi = \frac{(1 + 2.0 \times 10^4[M]}{(1 + 6.0 \times 10^4[M])\,(1 + 3.3 \times 10^2[M])}$$

In this case c must be $6.0 \times 10^4 M^{-1}$ and therefore the rate constants have the values (using $\omega = 1.2 \times 10^{11} M^{-1}s^{-1}$):

$k_s = 1.2 \times 10^8 s^{-1}$
$k_i^* = 2.4 \times 10^8 s^{-1}$
$k_t = 2.0 \times 10^6 s^{-1}$

Rate constants for the other wavelengths studied are given in Table 3. In every case, a good fit of the data to eqn. (16) can be obtained only when the dissociation rate constant for $^3B^*$ molecules, k_t, is assumed to be smaller than that for $^1B^*$ molecules, k_s.

TABLE 3

Rate constant for photodissociation and intersystem crossing at 25 °C

Excitation wavelength/nm	$k_i^*/10^8 s^{-1}$	$k_s/10^8 s^{-1}$	$k_t/10^6 s^{-1}$
254	100	30	27
297	5.0	2.1	3.6
313	2.4	1.2	2.0
334	1.1	0.52	8.6
366[a]	-	-	-

[a] See text.

The nature of a non-linear least squares analysis, however, is such that a fit can be obtained with a wide range of parameters, unless the data become nearly linear in part of the range. Such near linearity is found especially for the data at 297, 313 and 334 nm at high pressures, where presumably dissociation of $^3B^*$ is no longer competitive with collisionally induced relaxation to $^3B^0$. Equation (16) then can be reduced to the approximate form:

$$\frac{1}{\Phi} \cong \frac{c}{a} + \frac{bc}{a}[M] \tag{18}$$

or, with eqn. (17):

$$\frac{1}{\Phi} = 1 + \frac{k_i^*}{k_s} + \frac{\omega[M]}{k_s} \tag{19}$$

It can be seen from Fig. 1 that, in the high pressure region, where $1/\Phi$ becomes nearly linear in [M], the slope of that linear portion is a strong function of the excitation wavelength. Thus, k_s/ω increases with increasing photon energy, as is also shown in Fig. 4. The ratio k_s/k_i^*, as determined from the non-linear least squares analysis, does not vary significantly with wavelength. We conclude that intersystem crossing has about the same dependence on energy as dissociation. Data obtained in the luminescence studies and shown also in Fig. 4, correspond quite well with the present photochemical results.

It is apparent from Fig. 2 that the data at 366 nm do not fit the pattern established at the shorter wavelengths. Absorption at 436 and 405 nm populates exclusively the lowest excited singlet state [8] while absorption at wavelengths less than about 340 nm populates the second singlet state. When only the first singlet state is reached, the photochemical quantum yield is zero or extremely small, whereas energy dependent dissociation is found when the second excited state is exclusively populated. At the intermediate wavelength, 366 nm, both singlet states, one photoinert, the other photoactive, are populated by absorption. Unfortunately a quantitative treatment cannot be made because there are, in addition to the three rate constant parameters, a para-

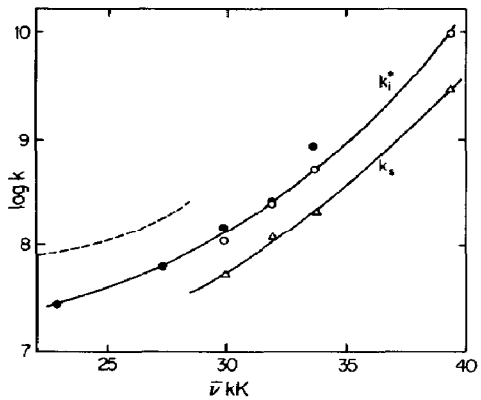

Fig. 4. Dependence of the intersystem rate constant, k_i^*, on total vibronic energy; ○, photochemical data; ●, luminescence data; of the photodissociation rate constant k_s (△); and of the total non-radiative rate constant for biacetyl [13] (----).

meter describing the faction of each state populated at 366 nm. It is only possible to state that with rate constants interpolated and extrapolated in Fig. 4 and with the assumption that the first and second excited singlet states are produced in the ratio of about one to three, respectively, at 366 nm, qualitative agreement with the experimental data is found.

The other parameter found from the data of Table 3 is the triplet dissociation rate constant, k_t. A clear trend with excitation wavelength cannot be established for k_t because of the uncertainty generated in the least squares analysis. In this analysis, k_t is large at 254 nm and decreases at longer wavelengths, but the value obtained at 334 nm does not fit this trend. Whether or not this behaviour is real we cannot be certain. It is true, however, that the low pressure quantum yields at 334 nm are larger than those at 313 nm (Fig. 2) well beyond the limits of experimental error.

The photoreactions of hexafluorobiacetyl originate only from the second excited singlet state and the vibrationally excited triplet state (it may, in fact, be the second triplet state, ^3B_g). Further, the rate of dissociation, certainly from the ^1A_u state, and perhaps as well that from the triplet state, is a strong function of the vibrational energy of the molecule (Fig. 4).

In addition, however, the rate of intersystem crossing is also strongly dependent on the excitation wavelength, and thus on the vibrational energy content of the excited molecule. Ware *et al.* [12] found a small increase, ~ 25%, in the total non-radiative rate constant of $^1B_{2u}$ state molecules of benzene for an increase in energy of 1500 cm^{-1}. More directly pertinent to our case are some measurements made by McClelland and Yardley [13] on the decay of fluorescence of biacetyl as a function of wavelength from 460 to 360 nm. Over this range, about 6000 cm^{-1}, all within the first excited singlet state, they observed an increase from 8×10^7 to 2×10^8 s^{-1} for the total rate of decay of the lowest $^1A_{1u}$ state. These data are reproduced in Fig. 4, so that they may be compared directly with our results. Other than a

displacement, their data on biacetyl fit well to our more extended data from photolysis and luminescence studies on the perfluoro derivative. We find that both intersystem crossing and photodissociation increase by several orders of magnitude as the energy is increased by 12,000 cm^{-1}. A similar effect for the total non-radiative rate constant for β-naphthylamine has been found by Schlag *et al.* [14].

Acknowledgement

The authors thank the National Research Council of Canada for a Grant in aid of research.

References

1 R. B. Cundall and A. S. Davies, Progr. React. Kinet., 4 (1967) 149.
2 G. F. Sheats and W. A. Noyes, Jr, J. Am. Chem. Soc., 77 (1955) 1421, 4532.
3 P. G. Bowers and G. B. Porter, J. Phys. Chem., 70 (1966) 1622.
4 A. S. Gordon, J. Chem. Phys., 36 (1962) 1660.
5 J. S. E. McIntosh and G. B. Porter, Trans. Faraday Soc., 64 (1968) 119.
6 C. S. Parmenter and H. M. Poland, J. Chem. Phys., 51 (1969) 1551.
7 J. S. E. McIntosh and G. B. Porter, to be published.
8 J. S. E. McIntosh and G. B. Porter, J. Chem. Phys., 48 (1968) 5475.
9 J. W. Sidman and D. S. McClure, J. Am. Chem. Soc., 77 (1955) 6461.
10 E. Drent and J. Kommandeur, Chem. Phys. Lett., 14 (1972) 321.
11 UBC Computing Centre Program BMDx85.
12 W. R. Ware, B. K. Selinger, C. S. Parmenter and M. W. Schuyler, Chem. Phys. Lett., 6 (1970) 342.
13 G. M. McClelland and J. T. Yardley, J. Chem. Phys., 58 (1973) 4368.
14 E. W. Schlag and H. von Weyssenhoff, J. Chem. Phys., 51 (1969) 2508.